A redox-active hybrid organic-inorganic polyoxometalate surfactant showed solvent-dependent self-assembly to form nano-scale architectures. The supramolecular assemblies exhibited contrasting electronic structure and redox activity to their molecular building units, and were found to be stable under electrochemical reduction and re-oxidation.

The development of new strategies to sustainably transform chemicals, harness solar energy and a range of other catalytic applications requires novel approaches to confine active materials in a controlled fashion. In this regard, hybrid organic-inorganic micellar and vesicular materials can exhibit enhanced functionality, tunability and stability (pH, redox and thermal) compared to purely organic systems,[1, 2] leading to potential applications in a wide range of catalytic processes.[2, 3] Organic-inorganic hybrid micellar assemblies have also been shown to act as templates in precise metal nanoparticle synthesis for energy storage and conversion applications.[4]

Polyoxometalates (POMs) are nanoscale molecular metal oxides, typically constructed from oxo-bridged W, Mo or V ions in their highest oxidation states.[5] They exhibit rich, reversible electrochemistry, excellent stability in acidic media and function as photo-oxidation catalysts for a wide range of organic transformations.[6, 7] Recently, they have also been shown to act as effective polar head groups in the formation of supramolecular organic-inorganic assemblies. POM-based micellar superstructures can be obtained *via* electrostatic self-assembly of negatively charged POMs and positively charged surfactant groups or organic polymers,[3, 8-11] ENREF 8 or through direct POM organofunctionalisation.[12] In this covalent approach, the inorganic POMs are functionalised with organic groups, such as long aliphatic alkyl chains, to form organic-inorganic hybrid molecules which can assemble to form micellar, vesicular and liquid crystal-like states. Polarz, Song, Cronin, Liu and their co-workers have pioneered the field of covalently functionalized polyoxometalate-surfactants, and shed light on their complex architectures and self-assembly,[13-24] ENREF 15 however, relatively little is known about the physicochemical properties of the nanoscale hybrid assemblies, and in particular the translation of POM functionality across the scales, from molecular to supramolecular and bulk.

Covalently hybridised POM surfactants offer several opportunities for development. Their composition, morphology and physical properties can be tuned not only through the chain length, conductivity and terminal functional groups of the organic ligand, but also through control of the shape, size, charge, photochemistry and electronic structure of the POM head group. It is thus possible to design molecular building blocks that will confer specific synergic properties to their organic-inorganic hybrid supramolecular assemblies.[25] A further consideration in the development of these systems is the nature (size, charge density and polarity) of the counter-cations of the POM-surfactants, which also plays a crucial role in the specific solubility of the compound.

We recently reported that the incorporation of organic moieties into the core of inorganic POMs *via* phosphonate linkers lowers the LUMO energy of the molecular metal oxide, and enhances its photosensitivity and photocatalytic activity.[26] To expand on this new concept, and probe the potential to translate the redox properties of molecular building units to supramolecular assemblies, we developed a redox-active hybrid POM with long aliphatic chains, and studied its solution state self-assembly behaviour and physicochemical properties (Figure 1). A Wells-Dawson-type-polyoxotungstate was selected as the inorganic surfactant head group due to its rich redox-chemistry and stability. The resultant material showed remarkable solvent-dependent self-assembly and the molecular and supramolecular phases exhibited contrasting electrochemical behaviour.

A POM surfactant was prepared by the condensation of (4-((11-mercaptoundecyl)oxy)phenyl)phosphonic acid with the mono-lacunary Dawson-type anion, $[P_2W_{17}O_{61}]^{10-}$ ($\{P_2W_{17}\}$) to give the hybrid POM, $H_6[P_2W_{17}O_{57}(H_{27}C_{17}O_4PS)_2]\cdot 3C_4H_9NO$ (H_6**1**) (see Figure 1) following our standard approach.[26] The chemical composition of H_6**1** was confirmed by elemental analysis (EA and ICP), ESI-MS, ^{1}H- and ^{31}P-NMR, FTIR and TGA (see SI).

Due to the excellent solubility of H_6**1** in polar aprotic solvents, *N*,*N*-dimethylformamide (DMF) was used for the bulk of the material characterisation. At concentrations up to the mM regime, dynamic light scattering (DLS) measurements identified no clear supramolecular aggregation in DMF, with the only particles falling into the hydrodynamic diameter (D_h) range of 0.5 to 4.8 nm. TEM analysis confirmed that individual POM-hybrid species were present (Figure S9).

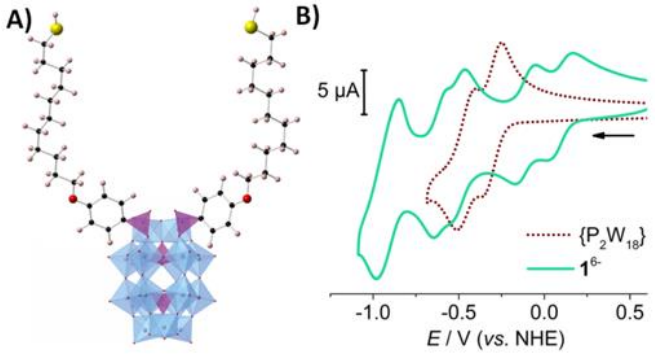

Figure 1. A) The molecular structure of H_6**1**. Color code: blue polyhedra = $\{WO_6\}$, purple polyhedra = $\{PO_4\}$ or $\{PO_3C\}$, red spheres = O, black = C, pink = H, yellow = S; B) The cyclic voltammograms of $\{P_2W_{18}\}$ and **1**$^{6-}$ collected vs. Fc/Fc^+ in DMF and converted to NHE.

The electrochemical redox-activity of **1**$^{6-}$ was examined in DMF using tetrabutylammonium hexafluorophosphate ($TBA\cdot PF_6$) as electrolyte. Figure 1B shows the cyclic voltammogram of **1**$^{6-}$ in DMF in comparison to its purely inorganic parent-anion $[P_2W_{18}O_{62}]^{6-}$ = $\{P_2W_{18}\}$. The first redox-process (corresponding to the reduction of **1**$^{6-}$ to **1**$^{7-}$) is shifted by *ca.* 400 mV towards more positive potentials compared to the equivalent process in $\{P_2W_{18}\}$. With regard to our previous findings,[26] and those of others,[27] this can be attributed to the electron-withdrawing effects of the phosphonate groups. Consequently, the LUMO is energetically lowered and the first redox process is shifted to a more positive potential.

After thorough drying under high vacuum at 70 °C overnight, H_6**1** was insoluble in deionized water at room temperature due

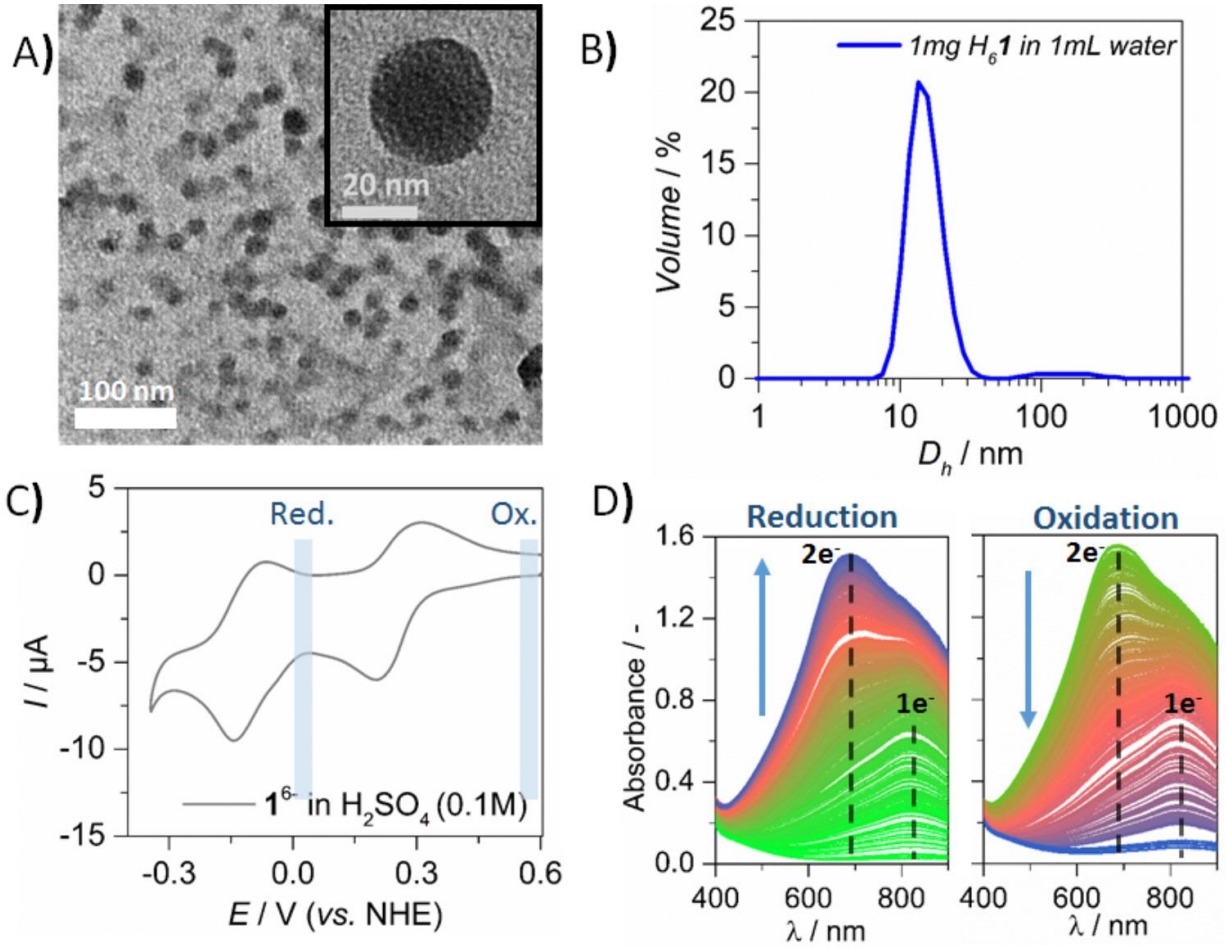

Figure 2. A) TEM images of supramolecular assemblies formed by H_6**1** in water after rapid heating to 70-80 °C; B) Particle size distribution curve determined from DLS for H_6**1** in water at 1 wt%; C) Cyclic voltammogram of 1.4 mM $\mathbf{1}^{6-}$ in 0.1M H_2SO_4 showing two broad redox processes associated with the reduction of the supramolecular aggregates and highlighting the potentials at which the reduction and oxidation processes were characterised spectroelectrochemically; D) Spectroelectrochemical analysis of the reduction and re-oxidation of a solution of 0.5 mM $\mathbf{1}^{6-}$ in 0.1M H_2SO_4.

to its long hydrophobic alkyl substituents. Upon rapid heating to temperatures of 70-80 °C, however, H_6**1** fully dissolved in water to form a clear, brown-orange solution, in stark contrast to the yellow colour observed in DMF solution. TEM analysis of the deposited solution of H_6**1** in water on a copper grid showed uniform spherical structures with diameters between 10 and 25 nm (Figure 2A), a size range that was supported by DLS measurements (Figure 2B).

To probe the electronic structure of the supramolecular hybrid-POM architectures, we investigated the electrochemical redox behaviour of $\mathbf{1}^{6-}$ (1.4 mM) in water with a 0.1 M H_2SO_4 electrolyte. DLS studies conducted on an equivalent solution showed aggregates with a mean hydrodynamic diameter D_h of 9 nm, indicative of small micellar assemblies (Figure S16). In our three-electrode set-up a glassy carbon electrode served as the working electrode, Ag/AgCl as reference electrode and Pt wire as the counter electrode. Two broad redox processes centred at $E_{1/2}$ = 0.26 V and $E_{1/2}$ = -0.11 V vs. NHE were observed (Figure 2C). For comparison, under identical conditions and at the same concentration as $\mathbf{1}^{6-}$, the cyclic voltammogram of $\{P_2W_{18}\}$ showed redox processes centred at 0.27 V and 0.10 V vs. NHE (Figure S14). Notably, the positive shift (compared to $\{P_2W_{18}\}$) of *ca.* 400mV seen for the first POM reduction potential of $\mathbf{1}^{6-}$ in DMF is absent in the aqueous H_2SO_4 solution. This contrasting redox behaviour may be due to intermolecular cooperativity or coulombic repulsion between metal oxide head groups in the supramolecular aggregates of $\mathbf{1}^{6-}$. To the best of our knowledge, this is the first time that the redox behaviour of micellar POM assemblies has been probed by cyclic voltammetry studies.

Potentiometric coulometry/bulk electrolysis measurements conducted on the aqueous sample indicate that the first broad redox-process of $\mathbf{1}^{6-}$, centred at 0.26 V *vs.* NHE, is a 2-electron process corresponding to a $\mathbf{1}^{6-}/\mathbf{1}^{8-}$ redox couple. Spectroelectrochemical analysis shows two maxima rising during bulk electrolysis at 0.05 V *vs.* NHE in the region between 600 and 900 nm. These two bands are characteristic POM-based intervalence charge transfer (IVCT) bands that correspond to the two-electron-reduced species (Figure 2D).[26] To probe the electrochemical stability of the micellar structures, absorption spectra were collected for the fresh (oxidised) sample in the absence of an applied potential, and spectroelectrochemical analysis (to 0.61 V *vs*. NHE) was performed to monitor the re-oxidation of the electrochemically reduced sample. The fresh sample showed no peaks in the range of 600 to 900nm, while those visible in the reduced sample rapidly disappeared as the POMs were re-oxidised. DLS measurements performed on the fresh sample, the reduced sample, and the re-oxidised sample showed that the particle size was retained across all samples,

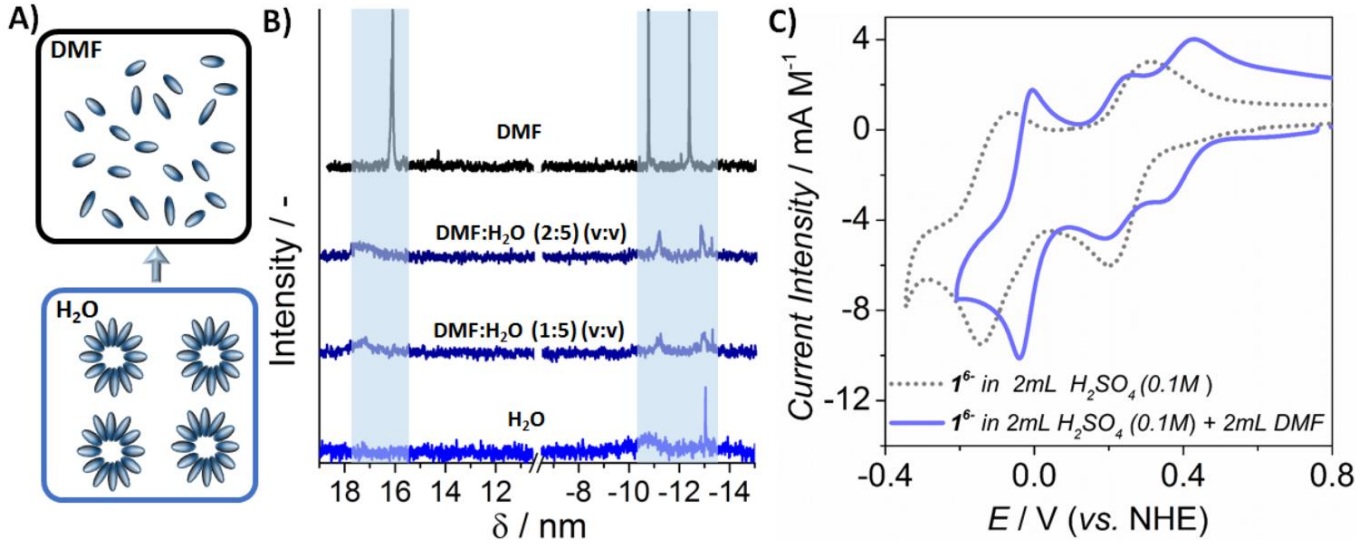

Figure 3. A) Schematic of the solvent-dependent supramolecular behaviour of H_6**1**; B) ^{31}P-NMR of aqueous solution of H_6**1** as DMF is added showing emergence of peaks as aggregates are disrupted. The top spectrum was obtained for H_6**1** in pure DMF; C) Voltammetric data for $\mathbf{1}^{6-}$ in aqueous initial phase (grey dotted line), and upon DMF addition (blue). The intensities are adjusted to compensate for the dilution.

indicating that the electrochemical behaviour was non-destructive to the supramolecular system (Figure S16). Cyclic voltammograms collected before and after bulk electrolysis at 0.05 V and after re-oxidation at 0.61 V *vs.* NHE showed that the $E_{1/2}$ values for the redox waves remained constant.

To further characterise the solution behaviour of H_6**1**, ^{31}P- and ^{1}H-NMR analyses were conducted. ^{31}P-NMR is an technique for the characterisation of organophosphonate-hybridised POMs, as it typically gives three clear, sharp, well-separated signals, two of which correspond to the two POM-templating phosphate (PO_4^{3-}) groups, and the other to the two equivalent organophosphonate (RPO_3^{2-}; R = organic moiety) groups. It was notable, therefore, that in D_2O the ^{31}P-NMR signals for H_6**1** were broad and at very low intensities compared to the signals that were observed in DMSO-d_6 and DMF-d_7 at similar concentrations. In contrast, corresponding measurements on $\{P_2W_{18}\}$ in D_2O give sharp signals (Figure S5). Furthermore, the alkyl chain signals were absent from the ^{1}H-NMR spectra (Figure S17). Stepwise addition of DMF-d_7 to the D_2O sample of H_6**1** led to the emergence of the signals in both the ^{1}H- and ^{31}P-NMR spectra (Figure 3B and S17). The lack of signals in the D_2O samples suggests that assembly of supramolecular aggregates causes blocking or shielding of the targeted nuclei. The growth of these signals upon DMF addition indicates dynamic solvent dependence of the supramolecular assembly process. Note that addition of further D_2O to the D_2O NMR sample led to no change in the spectra. Similar phenomena have been observed for thermosensitive block-copolymers,[28] where proton signals disappeared upon thermal stimulation and subsequent coiling of the polymer. Interestingly however, such behaviour has not been reported for other POM-surfactant systems to date.

To develop the observations made upon addition of DMF to the D_2O NMR sample, small volumes (up to 2mL) of DMF were added in a stepwise manner to a 2mL solution of $\mathbf{1}^{6-}$ in 0.1 M aqueous H_2SO_4. Cyclic voltammograms showed the gradual growth of two individually resolved redox processes at $E_{1/2}$ = 0.39 V and $E_{1/2}$ = 0.23 V *vs.* NHE, replacing the one broad redox process (centred at $E_{1/2}$ = 0.26 V *vs*. NHE) measured under purely aqueous conditions (Figure 3C). In addition, the second redox wave became increasingly sharp and reversible (ΔE_{pc} = 36 mV). The addition of less polar water-miscible solvents to an aqueous solution is expected to result in a negative shift in redox potentials.[29] Addition of DMF to the control sample, a 2mL solution of $\{P_2W_{18}\}$ in 0.1 M aqueous H_2SO_4, caused a negative shift in the POM redox waves, with the first process shifting from $E_{1/2}$ = 0.26 V to $E_{1/2}$ = 0.12 V vs NHE ($\Delta E_{1/2}$ = -0.14 V) (Figure S15). The positive shift of +0.13 V seen in the first redox process of $\mathbf{1}^{6-}$ therefore cannot be attributed to simple solvation effects. These observations allow us to draw two conclusions: firstly, that the addition of DMF to the aqueous system leads to the disruption of the supramolecular aggregates and allows recovery of molecular functionality, supporting our findings from the NMR experiments; and secondly, that the supramolecular aggregates have a remarkably different electronic structure (orbital energies) to the molecular building blocks. Our further studies will probe the relationship between the supramolecular and electronic structures of these organic-inorganic hybrid materials.

Conclusions

A novel redox-active surfactant POM (H_6**1**) was synthesised and its solvent-dependent self-assembly was investigated. In water, H_6**1** formed regular micellar assemblies, but addition of DMF led to the disruption of the supramolecular species. The aggregates were found to exhibit reversible redox chemistry, and contrasting electrochemical properties to those of their molecular building units. This transition from the molecular to

the supramolecular/nano regime and concomitant shift in physical properties opens the door to a wide range of environment-specific applications in catalysis, photo-catalysis, and advanced switchable materials. Future investigations will elucidate the self-assembly and solvent dependent dis-assembly of the system, and develop these next-generation redox-tunable soft materials as stable, water-soluble supramolecular capsules for applications in a wide range of organic solvent-free catalytic systems.

Acknowledgements

The authors gratefully acknowledge support from the EPSRC Directed Assembly Network, The University of Nottingham, the Nanoscale and Microscale Research Centre and The University of Nottingham's Advanced Molecular Material Research Priority Area. VS thanks the Faculty of Engineering at the University of Nottingham for the Dean Prize of Engineering. KK gratefully acknowledges the DAAD for financial support. AJK thanks the EPSRC Centre for Doctoral Training in Sustainable Chemistry (EP/L015633/1) for his studentship. EK gratefully acknowledges the Finnish Cultural Foundation (Suomen Kulttuurirahasto) for funding. The authors also thank Prof. Andrei Khlobystov for his help and advice on the TEM measurements.

Notes and references

1 T. Dwars, E. Paetzold and G. Oehme, *Angew. Chem. Int. Ed.*, 2005, **44**, 7174.
2 Q. Zhang, X.-Z. Shu, J. M. Lucas, F. D. Toste, G. A. Somorjai and A. P. Alivisatos, *Nano Lett.*, 2013, **14**, 379.
3 G. Maayan, R. Popovitz-Biro and R. Neumann, *J. Am. Chem. Soc.*, 2006, **128**, 4968.
4 M. Sasidharan, N. Gunawardhana, C. Senthil and M. Yoshio, *J. Mater. Chem. A*, 2014, **2**, 7337.
5 D.-L. Long, E. Burkholder and L. Cronin, *Chem. Soc. Rev.*, 2007, **36**, 105.
6 M. D. Tzirakis, I. N. Lykakis and M. Orfanopoulos, *Chem. Soc. Rev.*, 2009, **38**, 2609.
7 A. Dolbecq, P. Mialane, B. Keita and L. Nadjo, *J. Mater. Chem.*, 2012, **22**, 24509.
8 W. Bu, S. Uchida and N. Mizuno, *Angew. Chem. Int. Ed.*, 2009, **48**, 8281.
9 Y. Yan, H. Wang, B. Li, G. Hou, Z. Yin, L. Wu and V. W. Yam, *Angew. Chem. Int. Ed.*, 2010, **49**, 9233.
10 A. Nisar and X. Wang, *Dalton Trans.*, 2012, **41**, 9832.
11 H. Wang, Y. Yan, B. Li, L. Bi and L. Wu, *Chem. Eur. J.*, 2011, **17**, 4273.
12 A. Proust, B. Matt, R. Villanneau, G. Guillemot, P. Gouzerh and G. Izzet, *Chem. Soc. Rev.*, 2012, **41**, 7605.
13 S. Polarz, S. Landsmann and A. Klaiber, *Angew. Chem. Int. Ed.*, 2014, **53**, 946.
14 A. Klaiber, C. Lanz, S. Landsmann, J. Gehring, M. Drechsler and S. Polarz, *Langmuir*, 2016, **32**, 10920.
15 S. Landsmann, C. Lizandara-Pueyo and S. Polarz, *J. Am. Chem. Soc.*, 2010, **132**, 5315.
16 S. Landsmann, M. Luka and S. Polarz, *Nat. Commun.*, 2012, **3**, 1299.
17 A. Klaiber and S. Polarz, *ACS Nano*, 2016, **10**, 10041.
18 C. P. Pradeep, M. F. Misdrahi, F. Y. Li, J. Zhang, L. Xu, D. L. Long, T. Liu and L. Cronin, *Angew. Chem. Int. Ed.*, 2009, **48**, 8309.
19 S. Polarz, B. Smarsly and M. Antonietti, *ChemPhysChem*, 2001, **2**, 457.
20 W. Chen, D. Ma, J. Yan, T. Boyd, L. Cronin, D. L. Long and Y. F. Song, *ChemPlusChem*, 2013, **78**, 1226.
21 D. Li, J. Song, P. Yin, S. Simotwo, A. J. Bassler, Y. Aung, J. E. Roberts, K. I. Hardcastle, C. L. Hill and T. Liu, *J. Am. Chem. Soc.*, 2011, **133**, 14010.
22 C. G. Lin, W. Chen and Y. F. Song, *Eur. J. Inorg. Chem.*, 2014, **2014**, 3401.
23 J. Zhang, Y. F. Song, L. Cronin and T. Liu, *Chem. Eur. J.*, 2010, **16**, 11320.
24 J. Zhang, Y.-F. Song, L. Cronin and T. Liu, *J. Am. Chem. Soc.*, 2008, **130**, 14408.
25 A. Dolbecq, E. Dumas, C. R. Mayer and P. Mialane, *Chem. Rev*, 2010, **110**, 6009.
26 J. M. Cameron, S. Fujimoto, K. Kastner, R. J. Wei, D. Robinson, V. Sans, G. N. Newton and H. Oshio, *Chem. Eur. J.*, 2017, **23**, 47.
27 B. Matt, X. Xiang, A. L. Kaledin, N. Han, J. Moussa, H. Amouri, S. Alves, C. L. Hill, T. Lian and D. G. Musaev, *Chem. Sci.*, 2013, **4**, 1737.
28 E. V. Korchagina, X.-P. Qiu and F. M. Winnik, *Macromolecules*, 2013, **46**, 2341.
29 I. Persson, *Pure & Appl. Chem.*, 1986, **58**, 1153.